

**Table 1:** Patients who underwent VATS anatomical resection during this study period ( $n = 179$ )

Variables	No. of patients (%)
Age, median (years, range)	68 (26–87)
Sex	
Men	88 (49)
Women	91 (51)
Diagnosis	
Lung cancer	165 (92)
Metastatic lung tumour	6 (3)
Benign lung disease	8 (5)
Type of surgery	
Lobectomy	172 (96)
Right upper lobectomy	54
Right middle lobectomy	17
Right lower lobectomy	41
Right middle and lower lobectomy	2
Left upper lobectomy	37
Left lower lobectomy	21
Segmentectomy	7 (4)
Left S1+2-3	3
Right S3	1
Right S6	1
Left S4 + 5	1
Left S8-10	1
Preoperative 3D imaging	
Present	124 (69)
Absent	55 (31)

(96%) underwent lobectomy. This study involved 124 patients (69%) in whom 3D imaging was performed preoperatively and 55 patients (31%) in whom 3D imaging was not available because of contraindication to the use of contrast radiography (e.g., allergies to contrast medium, severe diabetes or bronchial asthma) or patient refusal against repeated imaging studies.

The characteristics and surgical outcomes of 124 patients undergoing 3D imaging are given in Table 2. There were 5 (4%) conversions from VATS to thoracotomy because of vessel bleedings. The frequency of patients presenting with complications with Grade 2 or above was 8% ( $n = 10$ ), and there were no 30-day or 90-day operative mortalities.

According to intraoperative findings, PA branches were precisely identified on the basis of preoperative 3D-CT imaging (Table 3) in 97.8% (309 of 316) of vessels and 94.4% (117 of 124) of patients. There were 7 patients with undetected PA branches including 5 right upper lobectomies (RULs) and 2 left upper lobectomies (LULs). Undetected PA branches were the truncus arteriosus superior in 3 patients, the ascending artery in 2 patients, and the apical artery and lingular artery in 1 patient each. A representative image of an undetected ascending artery is shown in Fig. 1. The actual sizes of the 7 missed branches in the 7 patients were all less than 2 mm. The 3D image findings in PA branches were identical to operative findings in cases other than upper lobectomy. The number of patients with anomalous or uncommon PA branching patterns was 15 (12%). A summary of the 3D image findings in patients with anatomical variants of the PA is given in Supplementary material, Table S1. All anomalous or uncommon PA branches were accurately confirmed by 3D imaging. Of the 26 patients receiving LUL, 5 patients (19%) had anatomical variants of mediastinal lingular branches of the PA, which included the A4 + A5 type and either the A4 or A5 type. In addition, there were 5 patients with lingular PA arising from the basilar artery, 2 patients with 2

**Table 2:** Patients who underwent VATS anatomical resection with the preoperative 3D imaging ( $n = 124$ )

Variables	No. of patients (%)
Age, median (years, range)	68 (35–87)
Sex	
Men	60 (48)
Women	64 (52)
Diagnosis	
Lung cancer	115 (93)
Metastatic lung tumour	5 (4)
Benign lung disease	4 (3)
Type of surgery	
Lobectomy	119 (96)
Right upper lobectomy	38
Right middle lobectomy	13
Right lower lobectomy	27
Right middle and lower lobectomy	1
Left upper lobectomy	26
Left lower lobectomy	14
Segmentectomy	5 (4)
Left S1 + 2-3	2
Right S6	1
Left S4 + 5	1
Left S8-10	1
Conversion from VATS to thoracotomy	5 (4)
Operative time, mean (min, range)	230 (132–444)
Bleeding, mean (ml, range)	110 (0–1406)
Postoperative complications (Grade $\geq 2$ )	
Present	10 (8)
Arrhythmia	3
Prolonged air leakage	2
Chylothorax	1
Bacterial pneumonia	1
Bleeding	1
Empyema	1
Recurrent nerve paralysis	1
Absent	114 (92)
30-day mortality	0
90-day mortality	0

superior segmental arteries coming directly from the main PA, 2 patients with double ascending arteries, 1 patient without an ascending artery and 1 patient with triple middle lobe branches (Fig. 2). The 3D imaging showed 5 patients with anomalous PVs (Supplementary material, Table S2).

We evaluated the relationship between various clinical factors and the occurrence of postoperative complications (Table 4) or overall operative time (Table 5) in 165 patients with primary lung cancer. Sex ( $P = 0.002$ ), pulmonary function test of forced expiratory volume in 1 s % (FEV1.0%;  $P = 0.011$ ), and the presence or absence of respiratory comorbidities including chronic obstructive pulmonary disease, interstitial pneumonia, bronchial asthma etc. ( $P = 0.018$ ) were found to be associated with the occurrence of complications. Conducting the preoperative 3D imaging tended to have associations, but the difference was not statistically significant ( $P = 0.054$ ). On multivariate logistic regression analysis for these statistically or marginally significant factors, male gender was shown to be the only statistically significant independent predictor (risk ratio: 5.432,  $P = 0.013$ , Hosmer–Lemeshow  $\chi^2$  test = 0.89,  $P = 0.641$ ), and 3D imaging also tended to be associated with the occurrence of complications (risk ratio: 2.852,  $P = 0.074$ ).

There were significant associations between total operative time (dichotomized at mean operative time, 237 min) and conducting

**Table 3:** Identification rate of the 3D imaging in pulmonary artery branches according to type of surgery

Variables	No. of patients (%)	No. of PABs involved in resection		Identification rate (%)		Undetected PABs (no. of patients)
		3D images	Surgical findings	A per-vessel basis	A per-patient basis	
Overall	124 (100)	309	316	97.8	94.4	1 mm (1)/2 mm (6)
Type of surgery						
Right upper lobectomy	38 (31)	84	89	94.4	86.8	1 mm (1)/2 mm (4)
Right middle lobectomy	13 (10)	24	24	100	100	-
Right lower lobectomy	27 (22)	55	55	100	100	-
Right middle and lower lobectomy	1 (1)	2	2	100	100	-
Left upper lobectomy	26 (21)	99	101	98.0	92.3	2 mm (2)
Left lower lobectomy	14 (11)	33	33	100	100	-
Segmentectomy	5 (4)	12	12	100	100	-
Uncommon PAB pattern	15 (12)	50	50	100	100	-

PABs: pulmonary artery branches.

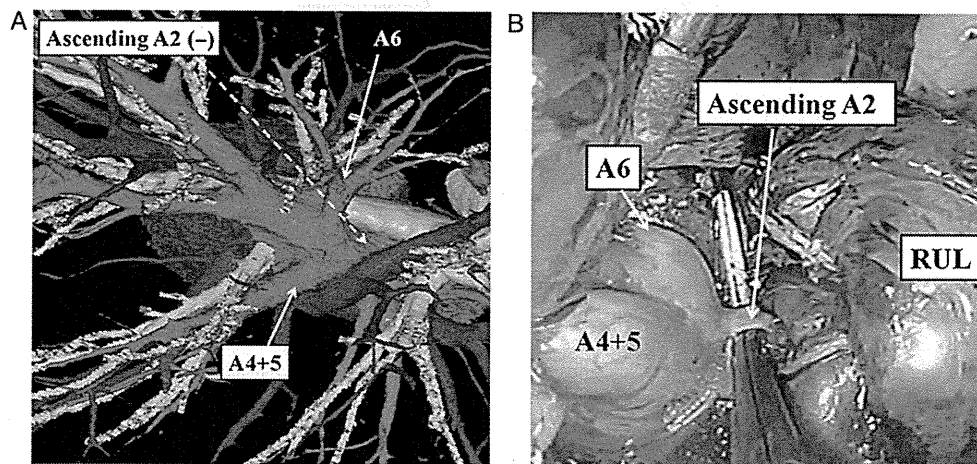


**Figure 1:** (A) A 3-dimensional computed tomographic image of the right pulmonary vessels. In this patient, a right upper lobectomy was performed. An ascending artery was not detected. (B) The intraoperative findings in this patient demonstrated the 2-mm ascending artery branches from the pulmonary artery.

the 3D imaging (risk ratio: 2.282,  $P=0.021$ ) and intraoperative blood loss (risk ratio: 1.005,  $P=0.005$ ) on univariate and multivariate analysis (Hosmer–Lemeshow  $\chi^2$  test = 5.92,  $P=0.656$ ).

## DISCUSSION

We set out to identify the effectiveness of 3D-CT imaging for pre-operative assessment of the branching patterns of pulmonary vessels and short-term surgical outcomes. A total of 97.8% of PA branches were precisely identified and all anomalous or uncommon PA and PV branching patterns were accurately confirmed by 3D imaging. In addition, patients undergoing preoperative 3D imaging tended to have lower incidences of postoperative complications and have significantly shorter operative time than those without the 3D simulations.

In reports in the literature concerning patients undergoing thoracoscopic and open surgery, 95–98% of PA branches were pre-operatively identified using 3D-CT angiography, similar to our results [10–12]. Several authors also studied anomalous PA, PV or bronchial variations for surgery using 3D reconstruction [9, 12–15]. 3D simulation is considered to be useful in performing anatomical

segmentectomy for small lung tumours for identifying the inter-segmental veins as boundary lines of the pulmonary segments in order to determine the surgical margins using lateral 3D images and to identify the target segmental bronchi using vertical 3D images before segmentectomy [8, 16, 17]. These reports show that intra-operative visual guidance of the target pulmonary vessels and bronchi, and their relationship to one another as revealed by high-quality 3D images, could help thoracic surgeons perform safer anatomical lung resection and be prepared for more complicated operations.

In our clinical experience with using the Synapse Vincent software, there have been advantages of the 3D system that are based on volume-rendering techniques. First, a surgeon without expert knowledge concerning synthetic imaging can quickly and easily construct 3D images of each patient. The mean processing time required to construct a 3D angiographic image is approximately 5 min. The 3D imaging also allows us to freely rotate the objects and change the dimensions of images. The virtual 3D-CT can provide an overview of the 3D relationships of the pulmonary vessel pathways and the tracheobronchial tree. Thus, it is employed for preoperative simulations, which also help educate trainees about surgical anatomy. Secondly, unlike the currently

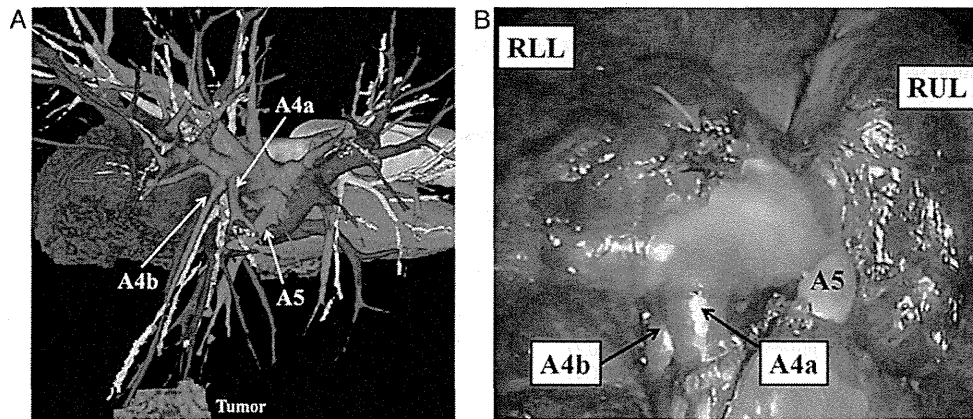


**Figure 2:** (A) The 3-dimensional computed tomographic image of the right pulmonary vessels showed that this patient had triple middle lobe pulmonary artery branches. (B) The intraoperative findings of this patient showed triple middle pulmonary artery branches corresponding to the 3-dimensional computed tomographic image.

**Table 4:** Association between clinical factors and the development of postoperative complications in patients who underwent VATS anatomical resection with primary lung cancer ( $n = 165$ )

Variables	Postoperative complications		Univariate analysis P-value	Multivariate analysis		
	Present	Absent		RR	95% CI	P-value
Overall	18	147				
Sex						
Men	15	65		5.432		
Women	3	82	0.002	1	1.427-20.683	0.013
Age, median (years, range)	69 (27-87)		0.46			
Clinical staging						
IA	11	104				
IB	5	28				
IIA	1	7				
IIB	1	3				
IIIA	0	4				
IIIB	0	1	0.81			
Tumour location						
Right upper lobe	4	47				
Right middle lobe	2	14				
Right lower lobe	4	35				
Left upper lobe	6	34				
Left lower lobe	2	17	0.87			
Preoperative 3D imaging						
Present	9	106		1		
Absent	9	41	0.054	2.852	0.904-8.999	0.074
FEV1.0%, median (% , range)	74 (44-89)		0.011	0.962	0.891-1.039	0.861
Operative procedure						
Lobectomy	18	143				
Segmentectomy	0	4	0.48			
Conversion from VATS to thoracotomy						
Present	0	6				
Absent	18	141	0.38			
Intraoperative blood loss, mean (ml, range)	112 (0-1406)		0.89			
Operative time, mean (min, range)	237 (131-455)		0.65			
Respiratory comorbidity						
Present	8	29		1.153	0.233-5.716	
Absent	10	118	0.018	1		0.25
Cardiovascular comorbidity						
Present	1	10	0.51			
Absent	17	137				
Diabetes						
Present	0	7	0.34			
Absent	18	140				

RR: risk ratio; CI: confidence interval; FEV1.0: forced expiratory volume in 1 s.

**Table 5:** Association between clinical factors and operative time (<237 min vs ≥237 min) in patients who underwent VATS anatomical resection with primary lung cancer (n = 165)

Variables	Univariate analysis, P-value	Multivariate analysis		
		RR	95% CI	P-value
Operative time, mean (min, range)	237 (132-455)			
Sex	0.26			
Age	0.15			
Clinical staging: IA/IB/IIA/IIB/IIIA/IIIB	0.25			
Tumour laterality: right/left	0.77			
Preoperative 3D imaging: present/absent	0.019	2.282	1.131-4.604	0.021
Conversion from VATS to thoracotomy: present/absent	0.77			
FEV1.0%	0.31			
Intraoperative blood loss	0.001	1.005	1.001-1.009	0.005
Operative procedure: lobectomy/segmentectomy	0.21			
Respiratory comorbidity: present/absent	0.08			
Cardiovascular comorbidity: present/absent	0.24			
Diabetes: present/absent	0.68			

RR: risk ratio; CI: confidence interval; FEV1.0: forced expiratory volume in 1 s.

available 3D-CT software programs, this system can show 3D images of the PA and the PV separately from the data of only one conventional CT scan. It can thereby reduce the radiation exposure dose. In contrast to the conventional method, we do not have to inject contrast media rapidly, and the infusion rate is sufficient at 1.5–2 ml/s. Consequently, we have not had any leakage accidents during contrast media infusion.

The disadvantages of 3D imaging include its potential deficiency in identifying bilateral upper lobe PA branches owing to the anatomically complex overlap of PA and PV branches. The ascending artery and truncus superior artery are often misidentified and confused with the apical segment vein or interlobar veins on 3D imaging. This might be due to the far more complicated ramification patterns of the PA in the upper lobe, particularly in the right upper lobe, than in the middle and lower lobes. However, we postulate that 3D imaging should be deemed acceptable because of the relatively low frequency of undetected PA branches.

The optimal strategy of managing postoperative complications of VATS anatomical resection is to prevent their occurrence. Perioperative complications and mortality with VATS lobectomy have been reported to occur at rates of ~5–32% and 0–7%, respectively [2, 18–20]. In the present study, postoperative complications in patients undergoing 3D imaging occurred in 8% with no mortality, and the risk of development of any complication in patients with 3D imaging was lower in comparison to those without 3D imaging. Notably, preoperative 3D simulation as well as intraoperative bleeding amount had significant association with total operative time. Possible reasons to explain these results are the assumptions that detailed surgical simulation and shared virtual lung anatomical information provided by 3D images between operating surgeons and a thoracoscopist might improve the safe and efficient performance of VATS, without causing vascular injuries due to unusual PA branching patterns, and thereby support a calm and efficient setting during lung resection.

The frequency of conversion from VATS lobectomy to open thoracotomy has been reported to range from 2% to as high as 23% [18, 19, 21, 22]. Although the most crucial concern with unexpected conversion to open thoracotomy are the possible increases in the risk of mortality and the development of complications, no

postoperative complications arose in our 5 patients undergoing the 3D-CT (date not shown). Depending on the skill and ability to predict which patients are more likely to require conversion, the occurrence of serious complications can often be avoided. 3D information will be useful in training surgeons learning VATS procedures by shared real-time imaging with an experienced surgeon, influencing a surgeon's learning curve.

The limitations of this study are its retrospective nature and potential bias. Patient selection bias in conducting the preoperative 3D imaging may influence the result of short-term benefits in adverse events and operative time. To truly show the benefits of 3D software, a prospective randomized trial is needed.

In conclusion, this study demonstrated that preoperative simulations using 3D-CT angiography for the assessment of pulmonary vessel branching patterns appear to be beneficial for the safe and efficient performance of VATS anatomical resection and for further understanding of the surgical anatomy related to general thoracic surgery. Further advances in 3D-CT imaging technology will be useful in the development of not only VATS and open thoracotomy, but also robotic surgeries and cognitive and technical surgical education systems, without exposing patients to unnecessary risks.

## SUPPLEMENTARY MATERIAL

Supplementary material is available at *EJCTS* online.

## ACKNOWLEDGEMENTS

The authors are indebted to the medical editors of the Department of International Medical Communications of Tokyo Medical University for their editorial review of the English manuscript.

## Funding

This study was supported by a Grant-in-Aid for Scientific Research, Japan Society for the Promotion of Science (24592104), and the Ministry of Education, Culture, Sports, Science and Technology, Japan.


**Conflict of interest:** The authors received fixed compensation for the described intellectual property without financial interest in its production, distribution or marketing.

## REFERENCES

- [1] Yim AP, Wan S, Lee TW, Arifi AA. VATS lobectomy reduces cytokine responses compared with conventional surgery. *Ann Thorac Surg* 2000;70:243–7.
- [2] Whitson BA, Andrade RS, Boettcher A, Bardales R, Kratzke RA, Dahlberg PS *et al.* Video-assisted thoracoscopic surgery is more favorable than thoracotomy for resection of clinical stage I non-small cell lung cancer. *Ann Thorac Surg* 2007;83:1965–70.
- [3] Port JL, Mirza FM, Lee PC, Paul S, Stiles BM, Altorki NK. Lobectomy in octogenarians with non-small cell lung cancer: ramifications of increasing life expectancy and the benefits of minimally invasive surgery. *Ann Thorac Surg* 2011;92:1951–7.
- [4] Swanson SJ, Meyers BF, Gunnarsson CL, Moore M, Howington JA, Maddaus MA *et al.* Video-assisted thoracoscopic lobectomy is less costly and morbid than open lobectomy: a retrospective multiinstitutional database analysis. *Ann Thorac Surg* 2012;93:1027–32.
- [5] Nakamura T, Koide M, Nakamura H, Toyoda F. The common trunk of the left pulmonary vein injured incidentally during lung cancer surgery. *Ann Thorac Surg* 2009;87:954–5.
- [6] Akiba T, Marushima H, Kamiya N, Odaka M, Kinoshita S, Takeyama H *et al.* Thoracoscopic lobectomy for treating cancer in a patient with an unusual vein anomaly. *Ann Thorac Cardiovasc Surg* 2011;17:501–3.
- [7] Ikeda N, Yoshimura A, Hagiwara M, Akata S, Saji H. Three dimensional computed tomography lung modeling is useful in simulation and navigation of lung cancer surgery. *Ann Thorac Cardiovasc Surg* 2013;19:1–5.
- [8] Saji H, Inoue T, Kato Y, Shimada Y, Hagiwara M, Kudo Y *et al.* Virtual segmentectomy based on high-quality three-dimensional lung modelling from computed tomography images. *Interact CardioVasc Thorac Surg* 2013;17:227–32.
- [9] Akiba T, Marushima H, Harada J, Kobayashi S, Morikawa T. Anomalous pulmonary vein detected using three-dimensional computed tomography in a patient with lung cancer undergoing thoracoscopic lobectomy. *Gen Thorac Cardiovasc Surg* 2008;56:413–6.
- [10] Fukuhara K, Akashi A, Nakane S, Tomita E. Preoperative assessment of the pulmonary artery by three-dimensional computed tomography before video-assisted thoracic surgery lobectomy. *Eur J Cardiothorac Surg* 2008;34:875–7.
- [11] Watanabe S, Arai K, Watanabe T, Koda W, Urayama H. Use of three-dimensional computed tomographic angiography of pulmonary vessels for lung resections. *Ann Thorac Surg* 2003;75:388–92; discussion 92.
- [12] Akiba T, Marushima H, Morikawa T. Confirmation of a variant lingular vein anatomy during thoracoscopic surgery. *Ann Thorac Cardiovasc Surg* 2010;16:351–3.
- [13] Ishikawa Y, Iwano S, Usami N, Yokoi K. An anomalous segmental vein of the left upper lobe of the lung: preoperative identification by three-dimensional computed tomography pulmonary angiography. *Interact CardioVasc Thorac Surg* 2012;15:512–3.
- [14] Akiba T, Morikawa T, Marushima H, Nakada T, Inagaki T, Ohki T. Computed Tomography Guided Thoracoscopic Segmentectomy for Lung Cancer with Variant Bronchus. *Ann Thorac Cardiovasc Surg* 2014;20:407–9.
- [15] Nakashima S, Watanabe A, Ogura K, Higami T. Advantages of preoperative three-dimensional contrast-enhanced computed tomography for anomalous pulmonary artery in video-assisted thoracoscopic segmentectomy. *Eur J Cardiothorac Surg* 2010;38:388.
- [16] Oizumi H, Kanauchi N, Kato H, Endoh M, Suzuki J, Fukaya K *et al.* Anatomic thoracoscopic pulmonary segmentectomy under 3-dimensional multidetector computed tomography simulation: a report of 52 consecutive cases. *J Thorac Cardiovasc Surg* 2011;141:678–82.
- [17] Shimizu K, Nakano T, Kamiyoshihara M, Takeyoshi I. Segmentectomy guided by three-dimensional computed tomography angiography and bronchography. *Interact CardioVasc Thorac Surg* 2012;15:194–6.
- [18] Walker WS, Codispoti M, Soon SY, Stamenkovic S, Carnochan F, Pugh G. Long-term outcomes following VATS lobectomy for non-small cell bronchogenic carcinoma. *Eur J Cardiothorac Surg* 2003;23:397–402.
- [19] McKenna RJ Jr, Houck W, Fuller CB. Video-assisted thoracic surgery lobectomy: experience with 1100 cases. *Ann Thorac Surg* 2006;81:421–5; discussion 25–6.
- [20] Lewis RJ, Caccavale RJ, Bocage JP, Widmann MD. Video-assisted thoracic surgical non-rib spreading simultaneously stapled lobectomy: a more patient-friendly oncologic resection. *Chest* 1999;116:1119–24.
- [21] Hennon M, Sahai RK, Yendamuri S, Tan W, Demmy TL, Nwogu C. Safety of thoracoscopic lobectomy in locally advanced lung cancer. *Ann Surg Oncol* 2011;18:3732–6.
- [22] Roviato G, Varoli F, Vergani C, Maciocco M, Nucca O, Pagano C. Video-assisted thoracoscopic major pulmonary resections: technical aspects, personal series of 259 patients, and review of the literature. *Surg Endosc* 2004;18:1551–8.

# Correlation between whole tumor size and solid component size on high-resolution computed tomography in the prediction of the degree of pathologic malignancy and the prognostic outcome in primary lung adenocarcinoma

Hisashi Saji<sup>1,4</sup>, Jun Matsubayashi<sup>2</sup>, Soichi Akata<sup>3</sup>, Yoshihisa Shimada<sup>1</sup>, Yasufumi Kato<sup>1</sup>, Yujin Kudo<sup>1</sup>, Toshitaka Nagao<sup>2</sup>, Jinho Park<sup>3</sup>, Masatoshi Kakihana<sup>1</sup>, Naohiro Kajiwara<sup>1</sup>, Tatsuo Ohira<sup>1</sup> and Norihiko Ikeda<sup>1</sup>

Acta Radiologica  
0(0) 1–9  
© The Foundation Acta Radiologica  
2014  
Reprints and permissions:  
sagepub.co.uk/journalsPermissions.nav  
DOI: 10.1177/0284185114554823  
acr.sagepub.com  


## Abstract

**Background:** The presence of ground glass opacity (GGO) on high-resolution computed tomography (HRCT) is well known to be pathologically closely associated with adenocarcinoma in situ.

**Purpose:** To determine whether it is more useful to evaluate the whole tumor size or only the solid component size to predict the pathologic high-grade malignancy and the prognostic outcome in lung adenocarcinoma.

**Material and Methods:** Using HRCT data of 232 patients with adenocarcinoma who underwent curative resection, we retrospectively measured the whole tumor and solid component sizes with lung window setting (WTLW and SCLW) and whole tumor sizes with a mediastinal window setting (WTMW).

**Results:** There was significant correlation between the WTLW and the measurements of pathological whole tumor (pWT) ( $r=0.792$ ,  $P<0.0001$ ). The SCLW and WTLW values significantly correlated with the area of pathological invasive component (pIVS) ( $r=0.762$ ,  $P<0.0001$  and  $r=0.771$ ,  $P<0.0001$ , respectively). The receiver operating characteristics area under the curve for WTLW, SCLW, and WTMW used to identify lymph node metastasis or lymphatic or vascular invasion were 0.693, 0.817, and 0.824, respectively. Kaplan-Meier curves of disease-free survival (DFS) and overall survival (OS) were better divided according to SCLW and WTMW, compared with WTLW. Multivariate analysis of DFS and OS revealed that WTMW was an independent prognostic factor (HR = 0.72, 95% confidence interval [CI] = 0.58–0.90,  $P=0.004$  and HR = 0.74, 95% CI = 0.57–0.96,  $P=0.022$ , respectively).

**Conclusion:** The predictive values of the solid tumor size visualized on HRCT especially in the mediastinal window for pathologic high-grade malignancy and prognosis in lung adenocarcinoma were greater than those of whole tumor size.

## Keywords

Lung adenocarcinoma, prognosis, solid component, ground glass nodule, high-resolution computed tomography

Date received: 19 May 2014; accepted: 17 September 2014

## Introduction

The National Lung Screening Trial demonstrated a significant reduction in mortality from lung cancer with low-dose CT screening of 20.0% (95% confidence interval [CI], 6.8–26.7;  $P=0.004$ ) (1). Recent advances in

<sup>1</sup>Department of Thoracic Surgery, Tokyo Medical University, Tokyo, Japan

<sup>2</sup>Department of Anatomic Pathology, Tokyo Medical University, Tokyo, Japan

<sup>3</sup>Department of Radiology, Tokyo Medical University, Tokyo, Japan

<sup>4</sup>Department of Chest Surgery, St. Marianna University School of Medicine, Kanagawa, Japan

## Corresponding author:

Hisashi Saji, MD, PhD Associate Professor Department of Chest Surgery, St. Marianna University School of Medicine 2-16-1 Sugao, Miyamae-ku, Kawasaki, Kanagawa 216-8511, Japan.  
Email: saji-q@ya2.so-net.ne.jp

high-resolution computed tomography (HRCT) and the widespread application of CT screening due to the positive results of screening CT trial have enhanced the discovery of small lung cancers, particularly adenocarcinoma (1). These often contain a non-solid component that presents as ground glass opacity (GGO) features on HRCT. Several investigators have reported that GGO is closely associated with bronchioloalveolar carcinoma (BAC) (2).

Recently, the International Association for the Study of Lung Cancer, the American Thoracic Society, and the European Respiratory Society proposed a new classification of lung adenocarcinoma. The terms BAC and mixed subtype adenocarcinoma are no longer used. For resected specimens, new concepts have been introduced such as adenocarcinoma in situ (AIS) and minimally invasive adenocarcinoma (MIA) for small solitary adenocarcinomas with either pure lepidic growth: AIS or predominantly lepidic growth with 5 mm invasion and MIA to define patients who, if they undergo complete resection, will have 100% or near 100% disease-specific survival rates, respectively (3,4). We therefore hypothesized that the GGO component is not related to malignancy or prognosis, implying that only the solid component of the tumor on HRCT (solid tumor size) is indicative of malignancy and prognosis in lung adenocarcinoma.

In this study, we first compared the whole tumor and solid component size, excluding areas of GGO, on preoperative HRCT with a lung window setting and whole tumor size with a mediastinal window setting with pathological whole tumor size and the area of pathologically confirmed invasion. We then determined whether it is more useful to evaluate the whole tumor size or that of only the solid component size to predict the degree of malignancy including lymph node involvement, lymphatic invasion, or vascular invasion of tumors in lung adenocarcinoma.

## Material and Methods

### Patients

Using preoperative HRCT data of 277 consecutive patients with adenocarcinoma who underwent curative surgical resection from January 2005 to December 2007, we retrospectively measured the whole tumor size and solid component size as follows: the whole tumor and solid component size was measured with lung window setting (WTLW and SCLW) and whole tumor size, with a mediastinal window setting (WTMW) on HRCT. Staging was determined according to the 7th edition of the TNM staging system (5). The histological tumor type was determined according to the World Health Organization (WHO) classification, 3rd edition.

In addition, we measured the maximum size of the area pathologically confirmed invasion for this study. We excluded 21 patients with adenocarcinoma with scattered invasive components for this analysis, due to difficulty in measuring not only the pathological invasive area but also the size of the solid component radiologically. Twenty-four patients with inappropriate tissue samples were also excluded following induction therapy or divided tumor resection due to intraoperative frozen diagnosis. Ultimately, 232 consecutive patients with adenocarcinomas were enrolled in this study. Radiological and pathological findings were conducted by SA and JP, and JM and TN, respectively, who were blinded from any clinical information.

Patients were examined at 3-month intervals for the first 2 years and at 6-month intervals for the next 3 years and thereafter on an outpatient basis. The follow-up evaluation involved the following procedures: physical examination, chest radiography, CT of the chest and abdomen, and blood examination, including that of pertinent tumor markers. Further evaluations, including brain magnetic resonance imaging or CT, bone scintigraphy and integrated positron emission tomography, were performed on the first appearance of any symptom or sign of recurrence. The median follow-up time of this series was 4.4 years.

### HRCT scanning

Chest images were obtained using 64-detector row CT scanners (LightSpeed VCT: GE Healthcare, Milwaukee, WI, USA and SOMATOM Sensation Cardiac 64: Siemens Medical Systems, Erlangen, Germany) and a 16-detector row CT scanner (BrightSpeed Elite: GE Healthcare, Milwaukee, WI, USA). High-resolution images of the tumors were acquired using the following parameters: 120 kV and auto exposure control; collimation, 0.6–1.25 mm; pitch, 0.9–0.984; 0.4–0.5 s per rotation; reconstructed interval, 1.25–1.5 mm; pixel resolution, 512 × 512; field of view, 20 cm; and a lung window settings (level = –500/width = 1500 HU) with high spatial frequency algorithm and mediastinal window settings (level = 40/width = 320 HU) with soft-tissue algorithm. GGO was defined as an increase in lung attenuation that did not obscure the underlying vascular markings. We defined the solid tumor size as the maximum dimension of the solid component of the lung windows excluding GGO (SCLW) or the maximum dimension of the whole tumor size of mediastinal setting (WTMW) (Fig. 1a and b).

### Pathological findings

Histopathological studies were performed according to WHO criteria, 3rd edition (6). All resected

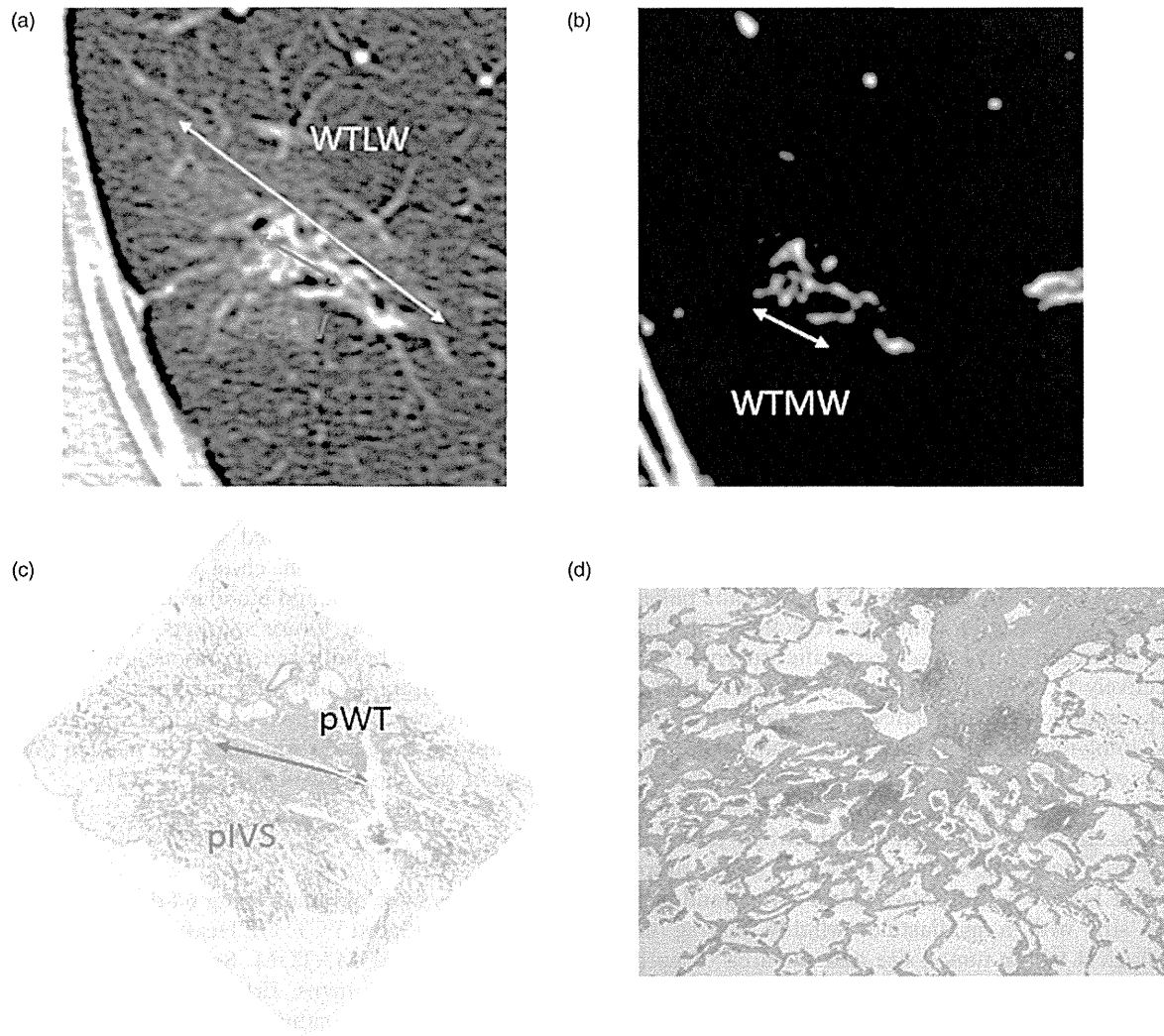


**Fig. 1.** Correlation between radiological and pathological findings in one typical case. WTLW and SCLW (a), WTMW (b), pWT and pIVS (c), pathological invasive area with high magnification (d). pIVS, pathologically confirmed invasion size; pWT, pathologically confirmed whole tumor size; SCLW, solid component size of lung windows setting; WTLW, whole tumor size of lung windows setting; WTMW, whole tumor size of mediastinal setting.

specimens were formalin-fixed and stained with hematoxylin and eosin in the routine manner. For detailed examinations of lymphatic or vascular invasion or pleural invasion, Elastica van Gieson stain was used to evaluate histological structure and tumor invasion. We also assessed several histological factors: (i) pathological nodal status (pN); (ii) vascular (v) or lymphatic (ly) invasion; and (iii) degree of tumor differentiation (well [G1], moderate [G2], poor [G3]). The maximum size of the pathological whole tumor (pWT) and of the pathological invasive component were measured (pIVS). The maximum size of pWT was assessed by standard gross measurement or histological reconstruction, as necessary. The maximum

size of the invasive component was measured microscopically. If the tumor was large, the maximum size of the invasive area was calculated by reconstruction of the tumor slides and measured (Fig. 1c and d). Pathologic high-grade malignancy was defined as lymph node involvement, lymphatic invasion, or vascular invasion.

#### Statistical analysis

The data are presented as numbers and percentages or mean  $\pm$  standard deviation, unless otherwise stated. The receiver operating characteristic curves of the whole and solid tumor sizes were used for the



**Table 1.** Radiological and pathological findings of 232 patients with lung adenocarcinoma.

Variables	n (% or range)	
Radiological findings		
WTLW: mean $\pm$ SD (cm)	2.59 $\pm$ 1.09 (0.73–6.84)	
SCLW: mean $\pm$ SD (cm)	2.01 $\pm$ 1.18 (0.00–5.78)	
WTMW: mean $\pm$ SD (cm)	1.87 $\pm$ 1.18 (0.00–5.71)	
Pathological findings		
pT status: pT1a / pT1b / pT2a / pT2b / pT3	86 (37.2) / 68 (29.2) / 61 (26.2) / 6 (2.7) / 11 (4.7)	
pN status: pN0 / pN1 / pN2	195 (83.7) / 20 (8.6) / 17 (7.7)	
pStage: pIA / pIB / pIIA / pIIB / pIIIA	141 (60.5) / 48 (20.6) / 8(3.4) / 8 (3.4) / 27 (12.1)	
pWT: mean $\pm$ SD, cm	2.61 $\pm$ 1.11 (0.90–7.20)	
pIVS: mean $\pm$ SD, cm	2.26 $\pm$ 1.27 (0.00–7.2)	
Differentiated: well or poorly	118 (50.6) / 107 (45.9)	ND: 8
Ly: positive / negative	127 (54.5) / 102 (43.8)	ND: 3
V: positive / negative	82 (35.2) / 150 (64.8)	

Ly, lymphatic invasion; ND, no data; pIVS, pathological invasion size; pN, pathological nodal status; pT, pathological T status; pWT, pathological whole tumor size; SCLW, solid component size of lung windows setting; V, vascular invasion; WTLW, whole tumor size of lung windows setting; WTMW, whole tumor size of mediastinal setting.

prediction of lymph node involvement, lymphatic invasion, or vascular invasion or well differentiation. We also performed multiple logistic regression analysis to determine the independent variables related to the whole tumor size and the solid tumor size for the prediction of the pathologic finding of high-grade malignancy. Overall survival (OS) was calculated from the date of surgery to the time of death. Observations were censored at final follow-up if the patient was living. Disease-free survival (DFS) was defined as the interval from the date of surgery until the first event (relapse or death from any cause) or the last follow-up visit. The duration of DFS was analyzed using the Kaplan-Meier method. Differences in OS or DFS were assessed using the log-rank test. To assess the potential independent and valuable prognostic effects of clinical tumor size on OS or DFS, we performed multivariate analysis with the Cox proportional hazards model using variables with  $P < 0.05$ . The data were statistically analyzed using the Statistical Package for Social Sciences software, version 10.5 (SPSS Inc., Chicago, IL, USA).

### Ethical considerations

The approval of the Institutional Review Board of Tokyo Medical University was obtained (project approval No. 1665), but as this was a retrospective study the need to obtain written informed consent from either the patients or their representatives was waived, in accordance with the American Medical Association Manual of Style (10th edition).

## Results

### Patient characteristics

There were 118 (51.0%) women and 114 (49.0%) men aged 35–86 years (mean, 65.0 years). The several radiological and pathological findings of 232 patients are summarized in Table 1.

### Correlation between radiological and pathological findings

Fig. 2 shows several correlations between radiological findings including WTLW, SCLW, or WTMW, and pathological findings including pWT or pIVS. There were significant correlations between SCLW and pIVS ( $R = 0.762$ , 95% CI = 0.702–0.811,  $P < 0.0001$ ), WTMW and pIVS ( $R = 0.771$ , 95% CI = 0.713–0.819,  $P < 0.0001$ ), and WTLW and pIVS ( $R = 0.792$ , 95% CI = 0.735–0.835,  $P < 0.0001$ ), respectively.

### Receiver operating characteristic curve

The receiver operating characteristic area under the curve values of WTLW, SCLW, WTMW, and pIVS used for predicting lymph node involvement, lymphatic invasion, vascular invasion, degree of differentiation, and pathologic high-grade malignancy (lymph node involvement or lymphatic or vascular invasion) are given in Table 2 and Fig. 3. The predictability of all outcomes on the basis of solid tumor size such as SCLW and WTMW was better than that using the

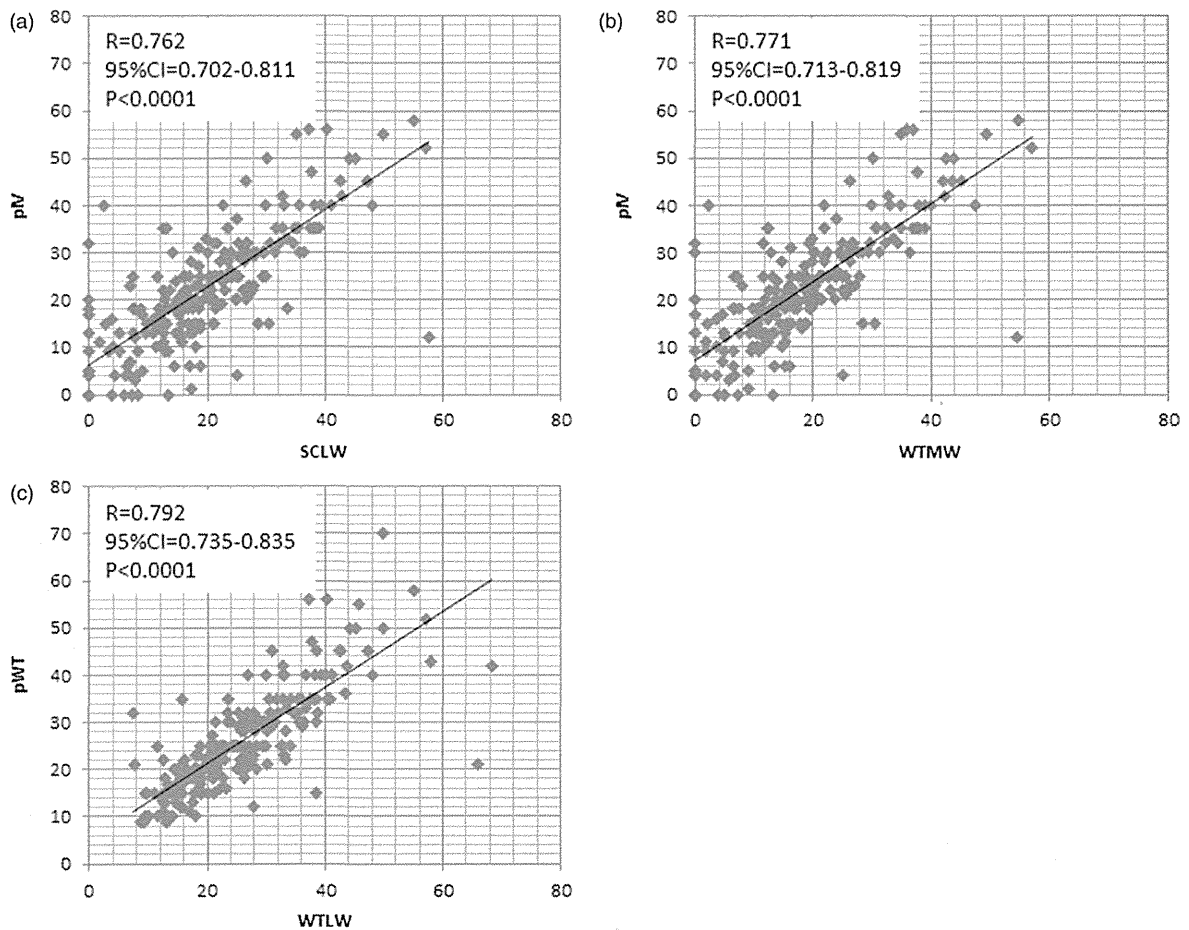


**Fig. 2.** Correlative graphs between radiological and pathological findings. There were significant correlations between SCLW and pIVS ( $R = 0.762$ ,  $95\% \text{ CI} = 0.702\text{--}0.811$ ,  $P < 0.0001$ ) (a), WTMW and pIVS ( $R = 0.771$ ,  $95\% \text{ CI} = 0.713\text{--}0.819$ ,  $P < 0.0001$ ) (b), and WTLW and pIVS ( $R = 0.792$ ,  $95\% \text{ CI} = 0.735\text{--}0.835$ ,  $P < 0.0001$ ) (c), respectively. pIVS, pathologically confirmed invasion size; pWT, pathologically confirmed whole tumor size; SCLW, solid component size of lung windows setting; WTLW, whole tumor size of lung windows setting; WTMW, whole tumor size of mediastinal setting.

**Table 2.** Receiver operative characteristic area under the curve values of WTLW, SCLW, WTMW, and pIVS used to predict pathologic findings.

Variable	WTLW		SCLW		WTMW		pIVS	
	AUC (95% CI)	P value	AUC (95% CI)	P value	AUC (95% CI)	P value	AUC (95% CI)	P value
pN	0.711 (0.625–0.797)	<0.0001	0.796 (0.723–0.870)	<0.0001	0.809 (0.737–0.880)	<0.0001	0.788 (0.717–0.859)	<0.0001
Ly	0.685 (0.616–0.754)	<0.0001	0.793 (0.735–0.852)	<0.0001	0.801 (0.744–0.859)	<0.0001	0.772 (0.711–0.833)	<0.0001
V	0.646 (0.593–0.719)	<0.0001	0.766 (0.704–0.828)	<0.0001	0.769 (0.706–0.831)	<0.0001	0.777 (0.717–0.837)	<0.0001
pN or Ly or V	0.693 (0.623–0.762)	<0.0001	0.817 (0.761–0.873)	<0.0001	0.824 (0.769–0.879)	<0.0001	0.796 (0.733–0.855)	<0.0001
Well diff.	0.623 (0.551–0.695)	0.001	0.770 (0.710–0.830)	<0.0001	0.771 (0.711–0.832)	<0.0001	0.770 (0.709–0.830)	<0.0001

Ly, lymphatic invasion; pIVS, pathological invasion size; pN, pathological lymph node status; SCLW, solid component size of lung windows setting; V, vascular invasion; Well diff., well differentiated; WTLW, whole tumor size of lung windows setting; WTMW, whole tumor size of mediastinal setting.

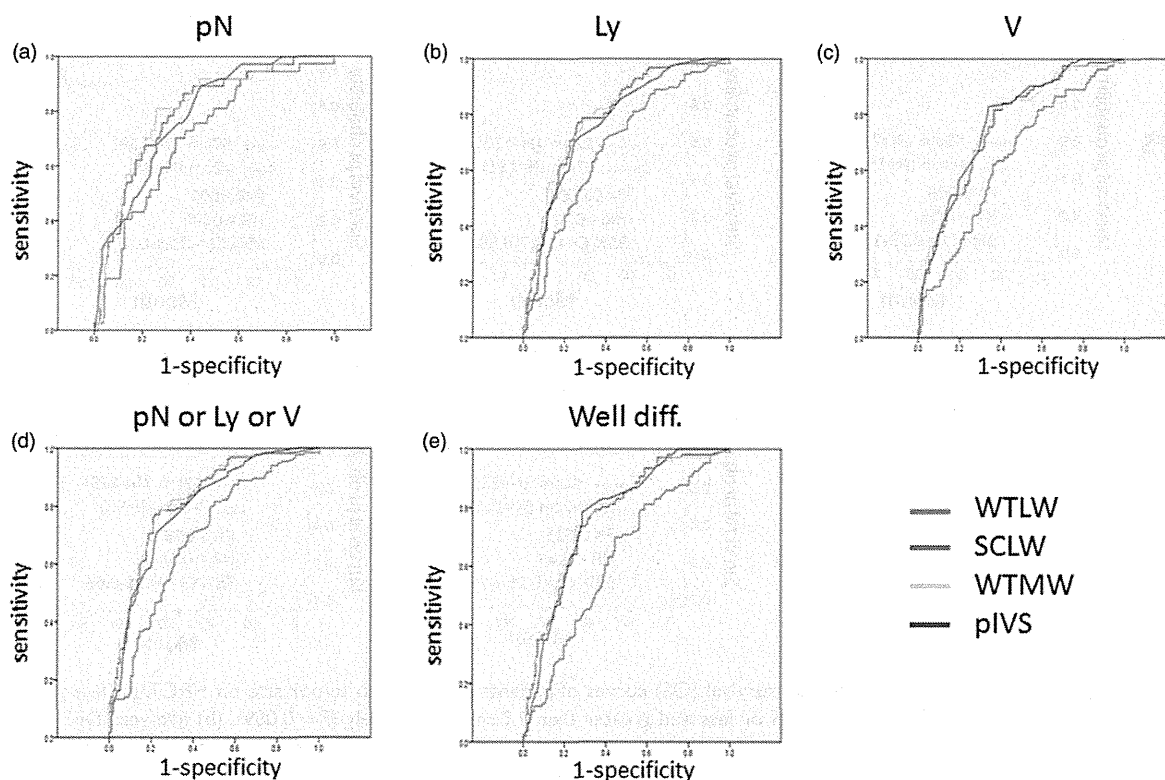


**Fig. 3.** Receiver operating characteristic area under the curve for detecting (a) pathological lymph node metastasis (pN), (b) lymphatic invasion (Ly), (c) vascular invasion (V), (d) high-grade malignancy (pN, VI, or PI), and (e) degree of differentiation for radiological whole and solid tumor sizes including WTLW, SCLW, and WTMW and pathological invasion area, pIVS. SCLW, solid component size of lung windows setting; WTLW, whole tumor size of lung windows setting; WTMW, whole tumor size of mediastinal setting.

whole tumor size that is WTLW for all subjects. The receiver operating characteristic curves of SCLW and WTMW were similar to that of pIVS that is pathological confirmed invasion area.

### Survival significance

We assessed survival significance of preoperative radiological findings including WTLW, SCLW, and WTMW. Patients were categorized into radiological measurement of tumor size greater than 2 cm or those 2 cm or less according to WTLW, SCLW, and WTMW. There were significant differences in both the DFS and OS of this series according to SCLW ( $P=0.0001$  and  $P=0.023$ ) and WTMW ( $P<0.0001$  and  $P=0.008$ ), respectively (Fig. 4). Moreover, to find the most valuable and independent radiological prognostic factor including WTLW, SCLW, and WTMW as a candidate of next T factor, we performed multivariate analysis of DFS and OS. Table 3 revealed that WTMW (HR=0.72, 95% CI=0.58–0.90,  $P=0.004$  and HR=0.74, 95% CI=0.57–0.96,  $P=0.022$ , respectively) was the independent prognostic factor among

preoperative variables among age, sex, WTLW, and SCLW in this series.

### Discussion

The frequency of identification of small lung cancers has increased since CT and enhanced scanning have become routine procedures. Small tumors, especially in lung adenocarcinomas, often contain GGO components as visualized on HRCT (2,7–9). Noguchi et al. first reported that type A and B small peripheral adenocarcinomas (localized bronchioloalveolar carcinoma without foci of active fibroblastic proliferation) showed no lymph node metastasis and a favorable prognosis (100% 5-year survival rate) (10). In 2011, new concepts were introduced including AIS and MIA. Because some of these cancers did not show growth for a long period, controversy remains as to how to manage subsolid nodules (11–14). Furthermore, both subsolid nodules and AIS have been discussed in relation to over diagnosis, which is defined as a diagnosis of lung cancer that would not lead to an individual's death because of the slow

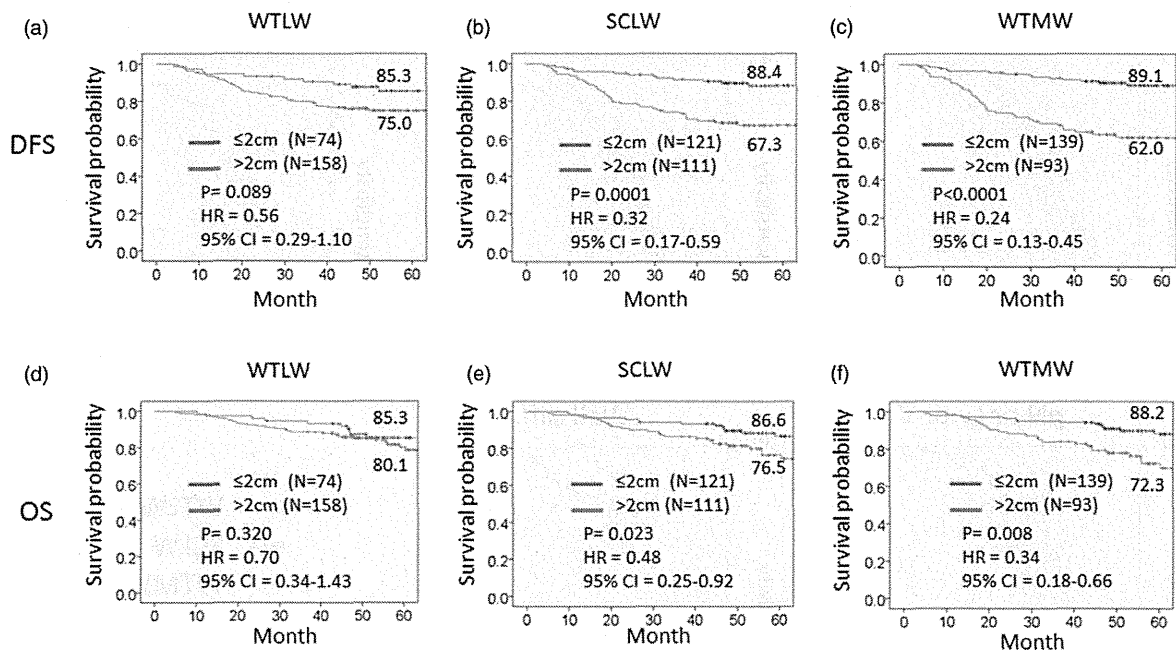


**Fig. 4.** Disease-free survival (DFS) and overall survival (OS) curves of patients according to tumor size on HRCT. (a) five-year DFS rate of 85.3% and 75.0% for a WTLW of 2.0 cm or less and greater than 2.0 cm, respectively ( $P=0.089$ ). (b) five-year DFS rate of 88.4% and 67.3% for a SCLW of 2.0 cm or less and greater than 2.0 cm, respectively ( $P=0.0001$ ). (c) five-year DFS rate of 89.1% and 62.0% for a WTMW of 2.0 cm or less and greater than 2.0 cm, respectively ( $P<0.0001$ ). (d) five-year OS rate of 85.2% and 80.1% for a WTLW of 2.0 cm or less and greater than 2.0 cm, respectively ( $P=0.320$ ). (e) five-year OS rate of 86.6% and 76.5% for a SCLW of 2.0 cm or less and greater than 2.0 cm, respectively ( $P=0.023$ ). (f) five-year OS rate of 88.2% and 72.3% for a WTLW of 2.0 cm or less and greater than 2.0 cm, respectively ( $P=0.008$ ). SCLW, solid component size of lung windows setting; WTLW, whole tumor size of lung windows setting; WTMW, whole tumor size of mediastinal setting.

**Table 3.** Multivariate analysis of DFS and OS.

Variable	Category	DFS			OS		
		HR	95% CI	P value	HR	95% CI	P value
Age (years)	<70						
	≥70	1.57	0.82–3.01	0.177	1.14	0.57–2.26	0.715
Sex	Men						
	Women	0.97	0.54–1.74	0.911	0.603	0.30–1.20	0.148
WTLW		0.94	0.89–1.00	0.040*	0.97	0.92–1.03	0.345
SCLW		0.82	0.66–1.01	0.067	0.80	0.62–1.03	0.078
WTMW		0.72	0.58–0.90	0.004*	0.74	0.57–0.96	0.022*

\*Statistically significant.

CI, confidence interval; DFS, disease-free survival; HR, hazard ratio; OS, overall survival; SCLW, solid component size of lung windows setting; WTLW, whole tumor size of lung windows setting; WTMW, whole tumor size of mediastinal setting.

growth rate and competing age-related risks for death (15–18).

The general concept of TNM classification by UICC is that “For consistency, in the TNM system, carcinoma in situ is categorized as Stage 0”, according to the 7<sup>th</sup> edition of the TNM Classification of Malignant

Tumours (19), which means AIS itself should not be used for staging grouping. However, clinical physicians specializing in lung cancer measure the tumor size by including the GGO components visualized on HRCT. On the basis of our hypothesis that the solid components, not the GGO components, of tumors as

visualized on HRCT, indicate malignancy and prognosis, we evaluated the role of solid tumor size (the size without the GGO component) in cases of lung adenocarcinoma.

First, we demonstrated that correlations between radiological findings including WTLW, SCLW, or WTMW, and pathological findings including pWT or pIVS. There were significant correlations between pIVS and SCLW or WTMW and between pWT and WTLW. Next we analyzed sensitivity and specificity of these radiological factors for predicting pathological malignant factors including lymph node involvement, lymphatic invasion, vascular invasion, and differentiation of the tumor. All receiver operating characteristic areas under the curves for predicting pN, Ly, V, high-grade malignancy (pN or Ly or V) and well differentiation were greater in the solid components size which is SCLW and WTMW than those for the whole tumor size which is WTLW. Because the range of mean radiological measurement of WTLW, SCLW and WTMW were from 1.87 to 2.59 cm in size and the cutoff point of 2 cm is also used as T factor. Finally, we analyzed each DFS and OS according to the cutoff point of 2 cm using whole and solid tumor sizes. Kaplan-Meier curves of both DFS and OS showed better division according to the solid components size, SCLW and WTMW, compared with the whole tumor size, WTLW. Moreover, multivariate analysis revealed that WTMW were identified as independent predictive factors for both DFS and OS. These results indicate that solid tumor size, not whole tumor size, more closely reflects the pathologic findings and those related to clinical tumor malignancy.

Several investigators have reported that the prognosis of patients with lung adenocarcinoma and a large GGO component visualized on HRCT was much better than that of patients with other adenocarcinoma types, irrespective of the maximal tumor dimension (20–23). In addition, JCOG0201, a multicenter prospective radiological study has examined the specificity, sensitivity, and accuracy of the radiologic diagnoses of lymphatic/vessel invasion and nodal involvement of clinical T1N0M0 adenocarcinoma made according to the HRCT findings (24). Recently, a multicenter registration study demonstrated that solid tumor size on HRCT and maximum standardized uptake values on PET/CT has greater predictive value for high-grade malignancy and prognosis in clinical stage IA lung adenocarcinoma than that of whole tumor size (25). This final result indicated that using the solid tumor size is much simpler than using the GGO ratio; furthermore, the solid tumor size can be applied to the T descriptor in the TNM classification.

In this study, patients with lung adenocarcinoma were eligible for assessment and approximately one-third of the patients with whole tumors greater than

3 cm were included in final analysis. This confirmation of the significance of using the solid component for prognosis is consistent with previous studies using small-sized lung adenocarcinoma. Therefore, this result suggested that this concept of using solid tumor size can be applied to the T descriptor of TNM classification for larger tumors.

To the best of our knowledge, this is the first study demonstrating the correlation between radiological and pathological findings and the prognostic significance of solid tumor size in lung adenocarcinoma including tumors larger than 3 cm. However, there are several limitations in this study. First, this was a medium-size retrospective, single-institution analysis. Second, to clarify and simplify measuring the radiological and pathological size, we excluded lung adenocarcinoma with scattered invasive components which were slightly less than 10% of the population. It remains unclear whether we should count the largest scattered invasive components or the sum total of them. Third, we used two radiological measurements, SCLW and WTMW, in this analysis. Our results suggested that using WTMW counting for solid invasive components might be a better mediator for prognostic outcome of lung adenocarcinoma compared with SCLW, which is consistent with some of the previous. It remains unclear whether WTMW or SCLW should be a better predictor. Therefore, larger and multicenter studies using identical protocols are needed.

In conclusion, the predictive values of solid tumor size visualized on HRCT especially in mediastinal windows for pathologic high-grade malignancy and prognosis in patients with lung adenocarcinoma were greater than those of the whole tumor size. We recommend that the solid tumor size be used to determine the T descriptor in the TNM classification of lung tumor and be defined as the true tumor size in cases of lung adenocarcinoma with a GGO component visualized on HRCT.

#### Acknowledgements

We are indebted to Professor James M. Vardaman of Waseda University and Professor J Patrick Barron, Chairman of the Department of International Medical Communications of Tokyo Medical University, for their editorial review of the English manuscript.

#### Conflict of interest

None declared.

#### Funding

This study was supported by a Grant-in-Aid for Scientific Research, Japan Society for the Promotion of Science (24592104), Ministry of Education, Culture, Sports, Science and Technology, Japan.

## References

1. Aberle DR, Adams AM, Berg CD, et al. Reduced lung-cancer mortality with low-dose computed tomographic screening. *N Engl J Med* 2011;365:395–409.
2. Nakata M, Sacki H, Takata I, et al. Focal ground-glass opacity detected by low-dose helical CT. *Chest* 2002;121:1464–1467.
3. Travis WD, Brambilla E, Noguchi M, et al. International Association for the Study of Lung Cancer/American Thoracic Society/European Respiratory Society: international multidisciplinary classification of lung adenocarcinoma: executive summary *Proc Am Thorac Soc* 2011;8:381–385.
4. Lee HJ, Goo JM, Lee CH, et al. Predictive CT findings of malignancy in ground-glass nodules on thin-section chest CT: the effects on radiologist performance. *Eur Radiol* 2009;19:552–560.
5. Goldstraw P, Crowley J, Chansky K, et al. The IASLC Lung Cancer Staging Project: proposals for the revision of the TNM stage groupings in the forthcoming (seventh) edition of the TNM Classification of malignant tumours. *J Thorac Oncol* 2007;2:706–714.
6. Travis WD, Brambilla E, Muller-Hermelink H, et al. World Health Organization Classification of Tumours: Pathology & Genetics Tumours of the Lung, Pleura, Thymus and Heart, 3rd edn. Lyon: IARC Press, 2004.
7. Okada M, Koike T, Higashiyama M, et al. Radical sublobar resection for small-sized non-small cell lung cancer: a multicenter study. *J Thorac Cardiovasc Surg* 2006;132:769–775.
8. Nakayama H, Yamada K, Saito H, et al. Sublobar resection for patients with peripheral small adenocarcinomas of the lung: surgical outcome is associated with features on computed tomographic imaging. *Ann Thorac Surg* 2007;84:1675–1679.
9. Suzuki K, Kusumoto M, Watanabe S, et al. Radiologic classification of small adenocarcinoma of the lung: radiologic-pathologic correlation and its prognostic impact. *Ann Thorac Surg* 2006;81:413–419.
10. Noguchi M, Morikawa A, Kawasaki M, et al. Small adenocarcinoma of the lung. Histologic characteristics and prognosis. *Cancer* 1995;75:2844–2852.
11. Kodama K, Higashiyama M, Yokouchi H, et al. Natural history of pure ground-glass opacity after long-term follow-up of more than 2 years. *Ann Thorac Surg* 2002;73:386–92; discussion 92–93.
12. Takashima S, Maruyama Y, Hasegawa M, et al. CT findings and progression of small peripheral lung neoplasms having a replacement growth pattern. *Am J Roentgenol* 2003;180:817–826.
13. Hiramatsu M, Inagaki T, Matsui Y, et al. Pulmonary ground-glass opacity (GGO) lesions-large size and a history of lung cancer are risk factors for growth. *J Thorac Oncol* 2008;3:1245–1250.
14. Sawada S, Komori E, Nogami N, et al. Evaluation of lesions corresponding to ground-glass opacities that were resected after computed tomography follow-up examination. *Lung Cancer* 2009;65:176–179.
15. Henschke CI, Yankelevitz DF, Mirtcheva R, et al. CT screening for lung cancer: frequency and significance of part-solid and nonsolid nodules. *Am J Roentgenol* 2002;178:1053–1057.
16. Toyoda Y, Nakayama T, Kusunoki Y, et al. Sensitivity and specificity of lung cancer screening using chest low-dose computed tomography. *Br J Cancer* 2008;98:1602–1607.
17. Jett JR. Limitations of screening for lung cancer with low-dose spiral computed tomography. *Clin Cancer Res* 2005;11:4988s–4992s.
18. Goo JM, Park CM, Lee HJ. Ground-glass nodules on chest CT as imaging biomarkers in the management of lung adenocarcinoma. *Am J Roentgenol* 2011;196:533–543.
19. Sobin LH, Gospodarowicz MK, Wittekind C. TNM Classification of Malignant Tumours. Oxford: John Wiley & Sons, Ltd., 2009.
20. Aoki T, Tomoda Y, Watanabe H, et al. Peripheral lung adenocarcinoma: correlation of thin-section CT findings with histologic prognostic factors and survival. *Radiology* 2001;220:803–809.
21. Suzuki K, Asamura H, Kusumoto M, et al. “Early” peripheral lung cancer: prognostic significance of ground glass opacity on thin-section computed tomographic scan. *Ann Thorac Surg* 2002;74:1635–1639.
22. Ohde Y, Nagai K, Yoshida J, et al. The proportion of consolidation to ground-glass opacity on high resolution CT is a good predictor for distinguishing the population of non-invasive peripheral adenocarcinoma. *Lung Cancer* 2003;42:303–310.
23. Tsutani Y, Miyata Y, Yamanaka T, et al. Solid tumors versus mixed tumors with a ground-glass opacity component in patients with clinical stage IA lung adenocarcinoma: Prognostic comparison using high-resolution computed tomography findings. *J Thorac Cardiovasc Surg* 2013;146:17–23.
24. Suzuki K, Koike T, Asakawa T, et al. A prospective radiological study of thin-section computed tomography to predict pathological noninvasiveness in peripheral clinical IA lung cancer (Japan Clinical Oncology Group 0201). *J Thorac Oncol* 2011;6:751–756.
25. Tsutani Y, Miyata Y, Nakayama H, et al. Prognostic significance of using solid versus whole tumor size on high-resolution computed tomography for predicting pathologic malignant grade of tumors in clinical stage IA lung adenocarcinoma: a multicenter study. *J Thorac Cardiovasc Surg* 2012;143:607–612.

# Clinical usefulness of gefitinib for non-small-cell lung cancer with a double epidermal growth factor receptor mutation

TAKEFUMI OIKAWA<sup>1</sup>, TATSUO OHIRA<sup>2</sup>, KEISHI OTANI<sup>2</sup>,  
MASARU HAGIWARA<sup>2</sup>, CHIMORI KONAKA<sup>1</sup> and NORIHIKO IKEDA<sup>2</sup>

<sup>1</sup>Chemotherapy Research Institute, Kaken Hospital, Ichikawa, Chiba 272-0827;

<sup>2</sup>Department of Surgery, Tokyo Medical University, Tokyo 160-0023, Japan

Received September 15, 2014; Accepted October 23, 2014

DOI: 10.3892/mco.2014.455

**Abstract.** The aim of this study was to investigate whether the pattern of epidermal growth factor receptor (EGFR) gene mutations affects sensitivity to gefitinib treatment. We investigated 44 surgically resected non-small-cell lung cancer (NSCLC) specimens obtained between 2001 and 2012 at the Tokyo Medical University Hospital. The specimens were obtained from patients treated with gefitinib as 1st-, 2nd-, or 3rd-line therapy for postoperative recurrent NSCLC. We detected EGFR mutations using the cycleave PCR technique. In addition, the specimens from non-responders were stained with antibodies against hepatocyte growth factor receptor (HGFR; MET) and hepatocyte growth factor (HGF). We assessed the progression of non-responders over a period of 2 months. Intermediate responders were considered to be patients who responded (exhibiting at least stable disease) to gefitinib therapy for 3-11 months, while long-term responders were defined as those who responded to gefitinib therapy for >12 months. The NSCLCs were histologically classified as 43 adenocarcinomas and one large-cell neuroendocrine carcinoma. One patient had an exon 18 point mutation, 23 an exon 19 deletion, 2 an exon 20 point mutation, 16 an exon 21 point mutation and 2 patients had both exon 20 and 21 point mutations. There were 4 non-responders, including the 2 patients with exon 20 mutation, 25 intermediate responders (including 10 patients under ongoing treatment) and 15 long-term responders (2 of whom are under ongoing treatment), including the 2 patients with both exon 20 and 21 mutations. Of the specimens obtained from non-responders, 3 stained with the anti-MET antibody and 1 stained with the anti-HGF antibody. Therefore, NSCLC with exon 20 mutation may respond to gefitinib treatment in the presence of an additional EGFR mutation.

## Introduction

Somatic mutations in the tyrosine kinase (TK) domain of epidermal growth factor receptor (EGFR) gene have been reported in patients with non-small-cell lung cancer (NSCLC). Certain mutations in the EGFR gene, such as leucine-to-arginine substitution at amino acid position 858 (L858R) in exon 21 or deletions in exon 19, are highly correlated with sensitivity to EGFR-TK inhibitors (TKIs) (1,2). The EGFR-TKIs gefitinib and erlotinib are effective in the treatment of EGFR-mutant NSCLC; however, there are also cases of EGFR-mutant NSCLCs exhibiting resistance to EGFR-TKI treatment. EGFR-TKIs have been shown to achieve a response in ~80% NSCLC patients with EGFR mutations, indicating that ~20% of NSCLC patients with EGFR mutation are unresponsive to this treatment (3).

A threonine-to-methionine substitution at amino acid position 790 (T790M) in exon 20 was reportedly associated with acquired resistance to EGFR-TKIs (4,5). In addition, hepatocyte growth factor receptor (HGFR; MET) gene amplification was reportedly associated with acquired resistance to EGFR-TKIs (6), while hepatocyte growth factor (HGF)-mediated MET activation was reported as the mechanism underlying EGFR-TKI resistance in lung cancer with EGFR-activating mutations (7). However, these studies were not pertaining to resistance, but rather investigating acquired resistance to EGFR-TKIs.

It was recently reported that pretreatment of NSCLC with T790M shortens the duration of response to EGFR-TKIs (9-12). However, over the last few years, we have observed long progression-free survival (PFS) in patients with T790M.

In this study, we aimed to investigate the pattern of EGFR mutations in NSCLC that affects sensitivity to EGFR-TKIs, determine the cause of shortened EGFR-TKI response duration and determine the correlation between resistance to EGFR-TKIs and phosphorylated MET or HGF expression.

## Materials and methods

**Patients and specimens.** We investigated 44 surgically resected NSCLCs between 2001 and 2012. The specimens were obtained from patients treated with gefitinib as 1st-, 2nd-, or 3rd-line therapy for postoperative recurrent NSCLC.

---

*Correspondence to:* Professor Norihiko Ikeda, Department of Surgery, Tokyo Medical University, 6-7-1 Nishi-shinjuku, Shinjuku-ku, Tokyo 160-0023, Japan  
E-mail: ikeda@wd5.so-net.ne.jp

**Key words:** double mutation, T790M, gefitinib, non-small-cell lung cancer

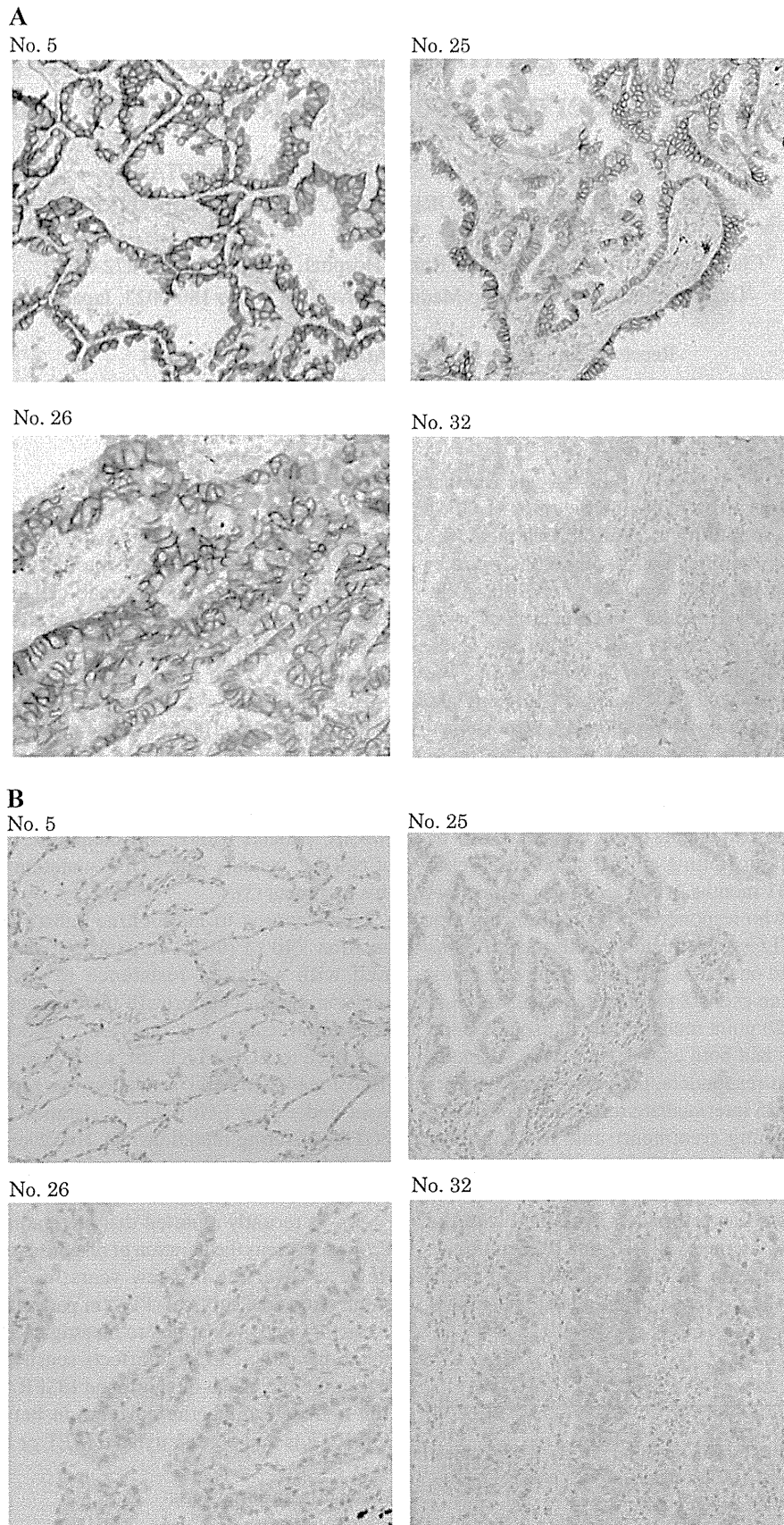


Figure 1. Immunohistochemical staining of non-small-cell lung cancer specimens. (A) The immunohistochemical staining for hepatocyte growth factor receptor (HGFR; MET) exhibited strong reactivity in the cell membranes of specimens no. 5, 25 and 26, whereas there was no reactivity with MET in specimen no. 32. (B) The immunohistochemical staining for HGF exhibited strong reactivity in the cell membranes of specimen no. 32, whereas there was no reactivity with HGF in specimens no. 5, 25, and 26.



Table I. Patient characteristics and response to gefitinib.

Patients	Gender	Age (years)	Histological type	Exon	Lobectomy	Response <sup>a</sup>
1	M	46	AdenoCa	18	Total	2
2	F	73	AdenoCa	19	Total	2
3	F	59	AdenoCa	19	Total	3
4	F	71	AdenoCa	19	Total	3
5	F	54	AdenoCa	19	Total	1
6	M	63	AdenoCa	19	Total	2
7	F	59	AdenoCa	19	Total	2
8	M	78	AdenoCa	19	Partial	2
9	F	68	AdenoCa	19	Partial	2
10	F	71	AdenoCa	19	Total	2
11	F	73	AdenoCa	19	Total	2
12	M	66	AdenoCa	19	Total	2
13	F	51	AdenoCa	19	Total	2
14	M	61	AdenoCa	19	Total	2
15	M	47	AdenoCa	19	Total	2
16	M	60	AdenoCa	19	Total	3
17	F	54	AdenoCa	19	Total	3
18	M	79	AdenoCa	19	Total	2
19	F	27	AdenoCa	19	Total	2
20	M	75	AdenoCa	19	Total	2
21	F	61	AdenoCa	19	Total	3
22	F	77	AdenoCa	19	Total	3
23	F	56	AdenoCa	19	Total	3
24	F	55	AdenoCa	19	Total	3
25	F	55	AdenoCa	20	Total	1
26	M	72	AdenoCa	20	Total	1
27	F	71	AdenoCa	21	Total	2
28	F	66	AdenoCa	21	Total	3
29	M	69	AdenoCa	20,21	Total	3
30	M	64	AdenoCa	20,21	Total	3
31	M	72	AdenoCa	21	Total	3
32	F	60	AdenoCa	21	Total	1
33	F	78	Large-cell Ca	21	Total	2
34	M	57	AdenoCa	21	Total	2
35	M	78	AdenoCa	21	Total	2
36	F	76	AdenoCa	21	Total	2
37	M	65	AdenoCa	21	Total	3
38	F	60	AdenoCa	21	Total	2
39	M	39	AdenoCa	21	Total	2
40	F	57	AdenoCa	21	Total	2
41	M	70	AdenoCa	21	Total	2
42	M	42	AdenoCa	21	Total	3
43	F	62	AdenoCa	21	Total	3
44	F	73	AdenoCa	21	Total	2

<sup>a</sup>1, No response; 2, intermediate response; 3, long-term response. M, male; F, female; Ca, carcinoma.

The NSCLCs were histologically classified as 43 adenocarcinomas and 1 large-cell neuroendocrine carcinoma. The patients included 19 men and 25 women, aged 27-78 years (mean age, 63.0 years).

*Immunostaining.* We detected EGFR mutations in matching formalin-fixed, paraffin-embedded tissue samples using the cycleave PCR technique (SRL Inc., Tokyo, Japan). We used an anti-MET rabbit monoclonal antibody (clone SP44;

Table II. Type of EGFR mutation and response to gefitinib.

Type of response	Type of mutation			
	Exon 18	Exon 19	Exon 20	Exon 21
Non-responders	0	1	2	1
Intermediate responders	1	14	0	10
Long-term responders	0	8	2 <sup>a</sup>	7 <sup>a</sup>

<sup>a</sup>Including 2 patients with both exon 20 and 21 mutations. EGFR, epidermal growth factor receptor.

cat no. 518-108830; Ventana Medical Systems, Inc., Tucson, AZ, USA) for MET staining and a goat polyclonal anti-human HGF antibody (cat no. 36073; LifeSpan BioSciences, Inc., Seattle, WA, USA) at a 1:40 dilution for HGF staining. Immunostaining for MET and HGF was performed using the Ventana System (Ventana Medical Systems, Inc, Harvard, MA, USA).

*Type of response to gefitinib.* We assessed the progression of non-responders to gefitinib treatment over a 2-month period. Intermediate responders included patients who responded (exhibiting at least stable disease) to gefitinib for 3-11 months. Long-term responders included patients who responded to gefitinib therapy for >12 months.

## Results

*EGFR mutations.* The 44 NSCLC specimens included 43 adenocarcinomas and one large-cell neuroendocrine carcinoma. There was 1 patient with an exon 18 point mutation, 23 with an exon 19 deletion, 2 with an exon 20 point mutation, 16 with an exon 21 point mutation and 2 with both exon 20 and 21 point mutations (Table I).

*Association of EGFR mutations with response to gefitinib.* There were 4 non-responders, including the 2 patients with exon 20 mutation, 25 intermediate responders (including 10 patients under ongoing treatment) and 15 long-term responders (2 of whom are under ongoing treatment), including the 2 patients with both exon 20 and 21 mutations (Table II).

*Immunostaining results.* We investigated MET and HGF immunostaining in 4 non-responders, 3 of whom were MET-positive and HGF-negative, whereas 1 patient was MET-negative and HGF-positive (Fig. 1).

## Discussion

Previous studies reported that the causes of acquired resistance to EGFR-TKIs in patients with EGFR mutations are a second mutation (T790M), MET amplification, or HGF-mediated MET activation. In those studies, ~50% of the cases with resistance to EGFR-TKIs exhibited a second mutation and ~20% were due to MET amplification (8). Our results were similar to those of previous studies, where EGFR-TKI therapy was the initial treatment. However, in our study, patients with NSCLC and exon 20 mutation responded to gefitinib in the presence of

an additional EGFR mutation. In particular, 2 cases (29 and 30) in this study were treated with gefitinib for 14 and 21 months, respectively. Our results were better in terms of PFS compared to those previously reported (2-13 months) (9-12).

Inukai *et al* reported that a small fraction of T790M-positive tumor cells at the beginning of treatment may lead to clinical gefitinib resistance as a result of the selective proliferation of T790M mutant cells (9). We therefore considered that the growth speed of T790M-positive cells and the number of T790M cells prior to EGFR-TKI treatment regulation were important for predicting PFS in patients with NSCLC and EGFR mutations. We considered that the T790M cell number was more important, rather than the T790M cell growth speed, as the latter is low (13). However, there is no established clinical method to quantitatively measure the number of T790M cells. Therefore, we must make a prediction based on the sensitivity of EGFR mutation testing in patients with NSCLC. The sensitivity of direct sequencing was previously found to be ~25%, that of cycleave PCR was ~5% and that of Scorpion ARMS was 1% (14).

The PFS of NSCLC patients, as assessed by direct sequencing in a study by Wu *et al* was 2 months (11). However, the PFS of NSCLC patients assessed using cycleave PCR in our study was 17.5 months. We attributed the longer PFS in our study to the detection of fewer T790M cells in our patients using more sensitive cycleave PCR prior to EGFR-TKI treatment.

Consequently, our findings suggest that NSCLC patients may be long-term responders if a double mutation is identified using a highly sensitive method, such as cycleave PCR or Scorpion ARMS.

Our data and previous reports taken together, indicate that NSCLC with exon 20 mutation will respond to gefitinib treatment in the presence of an additional EGFR mutation. However, further investigations are required to determine the mechanism underlying our findings.

## References

- Lynch TJ, Bell DW, Sordella R, *et al*: Activating mutations in the epidermal growth factor receptor underlying responsiveness of non-small-cell lung cancer to gefitinib. *N Engl J Med* 350: 2129-2139, 2004.
- Paez JG, Janne PA, Lee JC, *et al*: EGFR mutations in lung cancer: correlation with clinical response to gefitinib therapy. *Science* 304: 1497-1500, 2004.
- Inoue A, Suzuki T, Fukuhara T, *et al*: Prospective phase II study of gefitinib for chemotherapy-naïve patients with advanced non-small-cell lung cancer with epidermal growth factor receptor gene mutations. *J Clin Oncol* 24: 3340-3346, 2006.

4. Pao W, Miller VA, Politi KA, *et al*: Acquired resistance of lung adenocarcinomas to gefitinib or erlotinib is associated with a second mutation in the EGFR kinase domain. *PLoS Med* 2: e73, 2005.
5. Kobayashi S, Boggon TJ, Dayaram T, *et al*: EGFR mutation and resistance of non-small-cell lung cancer to gefitinib. *N Engl J Med* 352: 786-792, 2005.
6. Engelman JA, Zejnullahu K, Mitsudomi T, *et al*: MET amplification leads to gefitinib resistance in lung cancer by activating ERBB3 signaling. *Science* 316: 1039-1043, 2007.
7. Yano S, Wang W, Li Q, *et al*: Hepatocyte growth factor induces gefitinib resistance of lung adenocarcinoma with epidermal growth factor receptor-activating mutations. *Cancer Res* 68: 9479-9487, 2008.
8. Nguyen KS, Kobayashi S and Costa DB: Acquired resistance to epidermal growth factor receptor tyrosine kinase inhibitors in non-small-cell lung cancers dependent on the epidermal growth factor receptor pathway. *Clin Lung Cancer* 10: 281-289, 2009.
9. Inukai M, Toyooka S, Ito S, *et al*: Presence of epidermal growth factor receptor gene T790M mutation as a minor clone in non-small cell lung cancer. *Cancer Res* 66: 7854-7858, 2006.
10. Tokumo M, Toyooka S, Ichihara S, *et al*: Double mutation and gene copy number of EGFR in gefitinib refractory non-small-cell lung cancer. *Lung cancer* 53: 117-121, 2006.
11. Wu JY, Wu SG, Yang CH, *et al*: Lung cancer with epidermal growth factor receptor exon 20 mutations is associated with poor gefitinib treatment response. *Clin Cancer Res* 14: 4877-4882, 2008.
12. Su KY, Chen HY, Li KC, *et al*: Pretreatment epidermal growth factor receptor (EGFR) T790M mutation predicts shorter EGFR tyrosine kinase inhibitor response duration in patients with non-small-cell lung cancer. *J Clin Oncol* 30: 433-440, 2012.
13. Oxnard GR, Arcila ME, Chmielecki J, Ladanyi M, Miller VA and Pao W: New strategies in overcoming acquired resistance to epidermal growth factor receptor tyrosine kinase inhibitors in lung cancer. *Clin Cancer Res* 17: 5530-5537, 2011.
14. Pao W and Ladanyi M: Epidermal growth factor receptor mutation testing in lung cancer: searching for the ideal method. *Clin Cancer Res* 13: 4954-4955, 2007.

# Combination effect of photodynamic therapy using NPe6 with pemetrexed for human malignant pleural mesothelioma cells

SACHIO MAEHARA<sup>1</sup>, JITSUO USUDA<sup>2</sup>, TAICHIRO ISHIZUMI<sup>1</sup>, SHUJI ICHINOSE<sup>1</sup>, KEISHI OHTANI<sup>1</sup>, TATSUYA INOUE<sup>1</sup>, KENTARO IMAI<sup>1</sup>, HIDEYUKI FURUMOTO<sup>1</sup>, YUJIN KUDO<sup>1</sup>, NAOHIRO KAJIWARA<sup>1</sup>, TATSUYA OHIRA<sup>1</sup> and NORIHIKO IKEDA<sup>1</sup>

<sup>1</sup>Department of Surgery, Tokyo Medical University, Tokyo 160-0023;

<sup>2</sup>Department of Thoracic Surgery, Nippon Medical School, Tokyo 113-8603, Japan

Received September 9, 2014; Accepted October 17, 2014

DOI: 10.3892/ijo.2014.2746

**Abstract.** To identify a possible new treatment modality for malignant pleural mesothelioma (MPM), we examined whether combination treatment consisting of pemetrexed chemotherapy and photodynamic therapy (PDT) using the photosensitizer NPe6, enhanced the antitumor effect in both *in vitro* and *in vivo* models. We also investigated preclinical treatment schedules. Four human malignant mesothelioma cell lines (MSTO-211H, H2052, H2452 and H28) were assayed using the WST assay after treatment with pemetrexed and NPe6-PDT. The treatment schedule for the combination treatment was examined using nude mice. Pemetrexed pre-treatment enhanced the lethal effect of NPe6-PDT in the four malignant mesothelioma cell lines, but NPe6-PDT followed by pemetrexed treatment did not enhance cell lethality in the *in vitro* assay. Pemetrexed pre-treatment did not enhance the intracellular accumulation of NPe6, which is one of the determinants of the antitumor effect of PDT. In nude mice injected with MSTO-211H cells and then treated using a combination of pemetrexed and NPe6-PDT (10 mg/kg NPe6, 10 J/cm<sup>2</sup> laser irradiation), the tumor volume decreased by 50% but subsequently increased, reaching the pre-treatment value after 14 days. Pemetrexed treatment followed by NPe6-PDT resulted in an 80% reduction in the tumor size and inhibited re-growth. NPe6-PDT followed by pemetrexed treatment resulted in a 60% reduction in tumor size but did not inhibit re-growth. NPe6-PDT induced the expression of thymidylate synthase (TS), which confers resistance to pemetrexed, and NPe6-PDT followed by pemetrexed treatment did not enhance the treatment outcome *in vivo*. In conclusion, combination treatment, consisting of pemetrexed followed by

NPe6-PDT, should be further investigated as a new treatment modality for MPM. In the future, this combination treatment may contribute to a reduction in local recurrence and a prolonged survival period in patients with MPM.

## Introduction

Malignant pleural mesothelioma (MPM) is a locally aggressive disease characterized by a poor prognosis and an increasing incidence (1-4). MPM is difficult to detect at an early stage, and surgical and radiotherapeutic approaches are ineffective when used independently, because MPM spreads diffusely in the surrounding chest wall (5). No universally accepted treatment approach currently exists. An extrapleural pneumonectomy (EPP) with en bloc resection of the lung, pleura, ipsilateral diaphragm, and pericardium is one of the most invasive surgical procedures and is associated with a high risk of local recurrence (6,7). Recently, adjuvant radiation therapy to the ipsilateral hemithorax after EPP has been reported to result in a dramatic reduction in local relapse and the prolonged survival of patients with early-stage disease (8). Pemetrexed, a multi-target anti-folate, exhibits activity against various tumors, but especially against MPM and non-small cell lung cancer (NSCLC), for which it is routinely used (9). Pemetrexed inhibits at least three kinds of enzymes involved in folate metabolism, and in pyrimidine and purine biosynthesis: thymidylate synthase (TS), dihydrofolate reductase (DHFR), and glycinamide ribonucleotide formyltransferase (10). Combination of pemetrexed and cisplatin has become the standard first-line regimen for MPM based on the results of a phase III trial showing that this combination improved survival compared with cisplatin treatment alone (11). However, the impacts of induction chemotherapy using pemetrexed and cisplatin, and of adjuvant hemithoracic radiation therapy after EPP for MPM remain controversial (12). Flores *et al* reported that patients who underwent a pleurectomy/decortication had a better survival outcome than those who underwent EPP (13).

Photodynamic therapy (PDT) consists of the use of a tumor-specific photosensitizer and laser irradiation to induce the production of reactive oxygen species in cancer cells (14,15). This treatment modality is used for many

---

*Correspondence to:* Professor Jitsuo Usuda, Department of Thoracic Surgery, Nippon Medical School, 1-1-5 Sendagi, Bunkyo-ku, Tokyo 113-8603, Japan  
E-mail: jusuda@nms.ac.jp

**Key words:** malignant pleural mesothelioma, photodynamic therapy, pemetrexed, combination therapy